Pergamon

Chemical Engineering Science, Vol. 53, No. 24, pp. 4113–4127, 1998

Printed in Great Britain

PII: S0009–2509(98)000226–7

0009–2509/98/$–See front matter

Air entrapment and air bubble dispersion at two-dimensional plunging water jets

T. Brattberg and H. Chanson*

Department of Civil Engineering, The University of Queensland, Brisbane QLD 4072, Australia

(Received 17 September 1997; in revised form 6 July 1998; accepted 4 August 1998)

Abstract—Air–water bubbly flows are encountered in numerous engineering applications. One type of air–water shear flow, the developing flow region of a plunging jet, is discussed in the light of new experimental evidence. Distributions of air concentration and mean air–water velocity, and bubble chord length distributions are presented for inflow velocities ranging from 2 to 8 m/s. The results indicate that the distributions of void fraction follow closely analytical solutions of the diffusion equation, as developed by Chanson (1995a Report, CH46/95, pp. 368, 1997 Report CH48/97). In air–water shear layers, the velocity distributions have the same shape as in monophase flows but the characteristic parameters of the shear layer differ from monophase flow results, because of the interactions between the entrained air bubbles and the turbulence. © 1998 Elsevier Science Ltd. All rights reserved.

Keywords: Air bubble entrainment; Plunging water jet; Two-phase flow; Developing shear flow; Air bubble diffusion.

1. INTRODUCTION

1.1. *Presentation*

When a falling nappe impinges a pool of water, air may be entrained at the intersection of the jet with the receiving water (Fig. 1) and a large number of air bubbles may be advected within the turbulent developing shear flow. At a plunging jet, the near-flow field (next to and downstream of the impingement point) is characterised by a developing shear layer with some momentum transfer between the high-velocity jet core and the receiving pool of water, at rest at infinity. If air entrainment occurs, an air bubble diffusion layer takes place. The air diffusion layer may not coincide with the momentum shear layer, and the interactions between the momentum shear layer and the air diffusion layer contribute to the complexity of the air–water flow (Cummings and Chanson 1997a, b).

Plunging jet flow situations are encountered in chemical engineering plants for mixing and stirring chemicals (e.g. plunging jet columns, McKeogh and Ervine, 1981; Bin, 1993), in water treatment plants (e.g., Van de Donk, 1981), at drop structures along waterways, in cooling systems of power plants and in plunging breaking waves. A related case is the air entrainment associated with the continuous impingement of a solid surface into a liquid pool (e.g., Burley and Jolly, 1984). Despite numerous studies, the fluid mechanics of the air–water flow is not always well understood. It is the purpose of this study to detail systematically the air–water flow properties of the near field of two-dimensional plunging jets. The study extends the early investigations of Chanson (1995a) and Cummings (1996) (summarised in Cummings and Chanson, 1997a, b). Full details of the experimental data are reported in Chanson and Brattberg (1997).

1.2. *Bibliography*

Several researchers (e.g. review by Bin, 1993) showed interest in circular plunging jets and numerous experiments were performed with small circular jets (i.e. $\varnothing < 5$ mm) for which mostly qualitative studies of the air entrainment process were performed.

Only a small number of studies investigated the near-flow field below the impingement point: e.g., McKeogh and Ervine (1981), Van de Donk (1981), Bonetto and Lahey (1993), Chanson (1995a); and Cummings (1996). However, Bin (1993) and Chanson (1997) emphasised both the lack of information on the velocity profiles and air content distributions in the near-flow field.

2. EXPERIMENTAL APPARATUS AND INSTRUMENTATION

2.1. *Presentation*

The experimental apparatus was designed and used by Chanson (1995a) and Cummings (1996)

* Corresponding author. Tel.: 00 61 7 3365 3516; fax: +61 7 3365 4599; e-mail: h.chanson@mailbox.uq.edu.au.

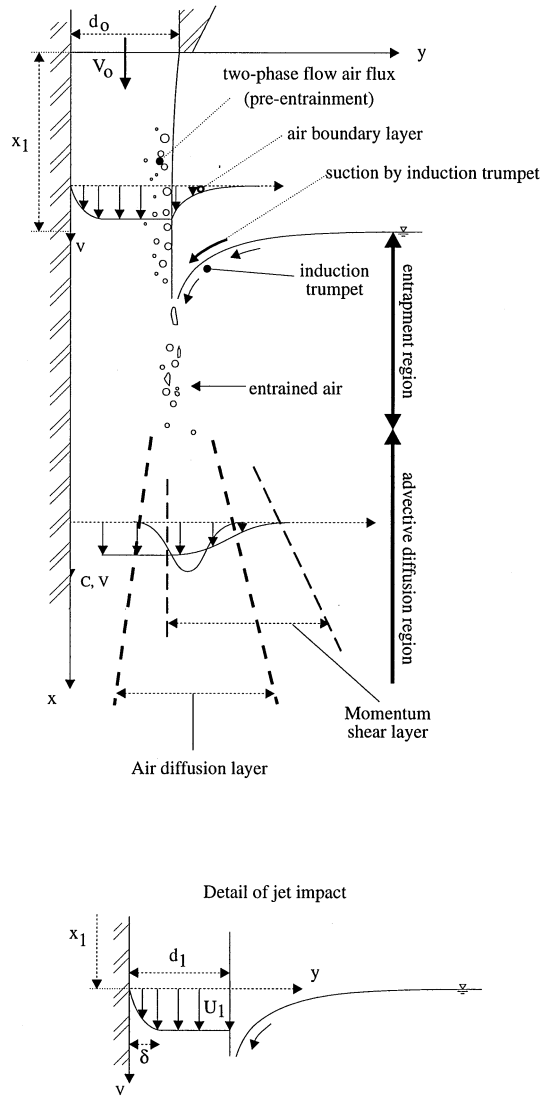

Fig. 1. Sketch of the plunging jet apparatus at the University of Queensland.

(Fig. 1, Table 1). It consists of a two-dimensional jet (0.269 m $\times$0.012 m at nozzle) plunging into a 0.3 m wide and 1.8 m deep pool. The jet support, made of 6 mm thick PVC, is 0.35 m long.

The displacement of the probes were controlled by two fine adjustment travelling mechanisms (made in-house) and the positions were measured with two Lucas Schaevitz Magnarules Plus™ (MRU-012 and MRU-036 in the normal and longitudinal directions, respectively). The specified accuracy of the Magnarules Plus is 0.01 mm. Each Magnarule Plus was calibrated in the Laboratory with a milli-machine Varnamo™ (Type U2-MM) and the error in the longitudinal and normal positions of the probes was less than 0.1 mm in each direction.

2.2. *Instrumentation*

Most air–water flow properties were recorded using a double-tip conductivity probe. The two tips, aligned in the direction of the flow, are identical with an internal concentric electrode ($\varnothing = 25$ μm, Platinum electrode) and an external stainless steel electrode of 200 μm diameter. Both tips were excited by an electronic system designed with a response time less than 10 μs. The measurements were recorded with a scan rate ranging from 20 to 40 kHz per channel.

Additional measurements in the free-falling jet were performed with a Pitot tube (external diameter $\varnothing = 3.3$ mm) connected to a pressure transducer (Validyne™ DP15) scanned at 500 Hz and a hot-film probe system. The hot-film probe system comprised a miniature conical film probe Dantec 55R42 (0.3 mm diameter film annulus) connected to a constant temperature anemometer.

2.3. *Inflow conditions*

The inflow was partially-developed: i.e., the turbulent boundary layer developing along the support could not be detected with the instrumentation (Pitot tube, hot-film probe) in most cases and $\delta/d_1 < 0.3$. The properties of the impinging jet and of its free-stream region were studied in detail by lowering the pool free-surface (to prevent interference from the pool). The turbulence characteristics of the 'potential flow' were recorded using the conical hot-film probe and the results (Table 2) suggest high levels of turbulence in the impinging free-stream. This is consistent with earlier observations recorded with a Pitot tube (Chanson, 1995a, Cummings, 1996) (Table 1, column 9).

Air concentration measurements, performed near the free-surface of the free-falling jet, indicated substantial aeration at the impinging jet free-surface (Table 2, column 11).

2.4. *Data collection and scatter*

All the air–water flow data were collected continuously while transverse probe displacement increments of about 0.1 mm were made. At each cross-section, the data are regrouped in 0.3 mm y-intervals. That is, in the Figs (e.g. Fig. 4), each data point represents the mean value (of C, V, F_{ab}) over an interval $\Delta y =$ 0.3 mm.

Note that, during the experiments, the free-surface level of the pool was fluctuating while the probes were attached to the channel. As a result, the data (e.g. Fig. 4) exhibit a greater scatter than the probe accuracy, reflecting the unsteady fluctuating nature of the investigated flow.

3. AIR ENTRAINMENT RATE

3.1. *Presentation*

At a plunging jet, air bubbles are entrained when the jet impact velocity U_1 exceeds a critical value V_e. For vertical supported plunging jets, Cummings and Chanson (1997a) observed $V_e = 2.0$ down to 1.1 m/s for jet turbulence intensity (at impact) from 0.3% up to 1.3%. Once air bubbles are entrained, two major

Table 1. Experimental investigations of two-dimensional plunging jet flows

Reference (1)	Run (2)	θ deg. (3)	Q_w (L/s) (4)	U_1 (m/s) (5)	d_1 (m) (6)	x_1 (m) (7)	Scanning rate (8)	Remarks (9)
Chanson (1995a)*		89						Supported jet ($W = 0.269$ m). Single-tip conductivity probe data.
	F1		6.46	2.36	0.0102	0.09	(*)	$Tu_1 = 0.017$
	F2		12.91	4.06	0.0118	0.09	(*)	$Tu_1 = 0.015$
	F3		19.37	5.89	0.0122	0.09	(*)	$Tu_1 = 0.0074$
	F4		25.82	8.0	0.012	0.09	(*)	
	F5		29.05	9.0	0.012	0.09	(*)	
Cummings (1996)		89						Supported jet ($W = 0.269$ m). Double-tip conductivity probe data.
	2m/s		6.46	2.39	0.010	0.0875	40 kHz	$Tu_1 = 0.016$
	6-m/s		19.37	6.14	0.0117	0.0875	40 kHz	$Tu_1 = 0.0075$
Present study		89						Vertical plunging jet ($W = 0.269$ m). Double-tip conductivity probe data.
	TBPJ-2		4.61	2.0	0.0090	0.10	20 kHz	
	TBPJ-3		8.56	3.0	0.0110	0.10	40 kHz	
	TBPJ-4-F50		12.51	4.0	0.0118	0.05	40 kHz	
	TBPJ-4		12.10	4.0	0.0116	0.10	40 kHz	
	TBPJ-4-F150		11.67	4.0	0.0114	0.15	40 kHz	
	TBPJ-5		15.49	5.0	0.0119	0.10	40 kHz	
	TBPJ-6		18.83	6.0	0.0120	0.10	40 kHz	
	TBPJ-7		22.14	7.0	0.0121	0.10	40 kHz	
	TBPJ-8		25.43	8.0	0.0121	0.10	40 kHz	

Note: d_1: impact jet thickness; Tu_1: turbulence intensity of the impinging jet; U_1: free-stream velocity at impact; x_1: fall height; θ: jet angle with horizontal; (*): analogue integration.

Table 2. Plunging jet experiments: characteristics of the free-falling impinging jets (Present study)

Run	V_0 (m/s)	d_0 (m)	x_1 (m)	d_1 (m)	U_1 (m/s)	V_e (m/s) (*)	Tu_1 (†)	Sk_1 (†)	Ku_1 (†)	$(q_{air}/q_w)_1$	Remarks
(1)	(2)	(3)	(4)	(5)	(6)	(7)	(8)	(9)	(10)	(11)	(12)
TBPJ-2	1.43	0.012	0.10	0.0090	2.0	1.1	0.0173	0.00025	11.4	0.11	$W = 0.269$ m
TBPJ-3	2.65	0.012	0.10	0.0110	3.0	1.1	0.0265	0.00020	15.0	0.14	
TBPJ-4-F50	3.88	0.012	0.05	0.0118	4.0	1.1	0.02	0.00015	12.0	0.08	
TBPJ-4	3.75	0.012	0.10	0.0116	4.0	1.1	0.0285	0.00036	9.93	0.17	
TBPJ-4-F150	3.62	0.012	0.15	0.0114	4.0	1.1	0.03	0.00070	11.0	0.24	
TBPJ-5	4.80	0.012	0.10	0.0119	5.0	1.1	0.025	0.00033	8.14	0.20	
TBPJ-6	5.83	0.012	0.10	0.0120	6.0	1.1	—	—	—	0.18	
TBPJ-7	6.86	0.012	0.10	0.0121	7.0	1.1	—	—	—	0.22	
TBPJ-8	7.88	0.012	0.10	0.0121	8.0	1.1	—	—	—	0.21	

Notes: d_0: nozzle thickness; d_1: impact jet thickness; Ku_1: kurtosis factor of the impinging jet; q_{air}: quantity of entrained air at the free-surface of the impinging jet; Sk_1: skewness factor of the impinging jet; Tu_1: turbulence intensity of the impinging jet; U_1: free-stream velocity at impact; V_0: nozzle velocity; W: jet width; x_1: fall height.
*Cummings (1996). †hot-film probe data measured in the free-stream at $y/d_1 = 2/3$; (—): information not available.

air entrainment process may be observed (Chanson and Cummings, 1994a; Chanson, 1997).

For low velocities (i.e. $U_1 < 2$ m/s), air entrainment is caused by the pool of water being unable to follow the undulations of the jet surface and small air pockets are formed. The entrapment process is intermittent and pulsating, with the entrainment of individual bubbles and elongated air packets (e.g., Chanson and Brattberg, 1996).

At larger jet impact velocities (i.e. $U_1 > 3$ to 5 m/s for the present study), a qualitative change in the air entrainment process is observed. An air layer is set into motion by shear forces at the surface of the jet and enters the flow, forming an air cavity. Air pockets are entrained by intermittent releases at the lower end of the air cavity in the form of elongated pockets (Chanson and Cummings, 1994a).

3.2. *Quantity of entrained air*

The quantity of entrained air was calculated from the distributions of air concentration C and air–water velocity V:

$$q_{air} = \int_0^{+\infty} C^* V \, dy \tag{1}$$

where y is the distance normal to the jet support, and C and V were measured below the impingement point (i.e. $x > x_1$). Equation (1) is basically the continuity equation for air.

During the present series of experiments, the dimensionless air flow rate q_{air}/q_w was observed to be a constant independent of the longitudinal distance from the entrainment point $(x - x_1)$, for given inflow conditions (i.e. d_1, U_1, x_1 fixed), and for $(x - x_1) < 0.2$ m. No air detrainment was observed for $(x - x_1)/d_1 < 17$.

Experimental results (Fig. 2) indicate that the quantity of entrained air increases with increasing jet impact velocity for a constant fall height. The data show also a drastic change in the rate of increase for $U_1 \sim 4$ m/s. Several authors (e.g., Van de Sande and Smith, 1973; Sene, 1988) observed the same trend and it is believed to be related to a change of air entrainment mechanism (Bin, 1993; Chanson, 1997).

The effect of the fall height on the quantity of entrained air was studied for one jet impact velocity ($U_1 = 4$ m/s). The results show a linear increase of quantity of entrained air with increasing fall height (i.e., $q_{air} \propto x_1$). As a comparison, several authors suggested: $q_{air} \propto (x_1)^{0.4 \text{ to } 0.65}$ with thin circular jets (Bin, 1993).

Overall the data are best correlated by

$$\frac{q_{air}}{q_w} = 7.7\text{E}-4^* \left(\frac{x_1}{d_1} - 1.04 \right)^* \left(\frac{U_1 - V_e}{\sqrt{g^* d_1}} \right)^{1.8}$$

$$\text{for } V_e \leqslant U_1 \leqslant 4 \text{ m/s} \tag{2A}$$

$$\frac{q_{air}}{q_w} = 2.0\text{E}-3^* \left(\frac{x_1}{d_1} - 1.04 \right)^* \left(\frac{U_1 - V_e}{\sqrt{g^* d_1}} + 9.3 \right)$$

$$\text{for } 4 \leqslant U_1 \leqslant 8 \text{ m/s} \tag{2B}$$

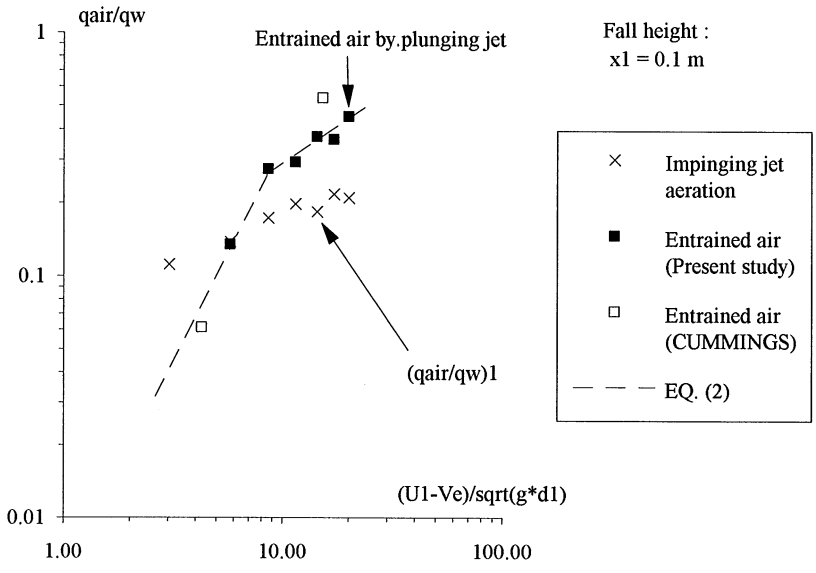

Fig. 2. Dimensionless quantity of entrained air q_{air}/q_w as a function of the dimensionless impact jet velocity $(U_1 - V_e)/\sqrt{g*d_1}$ - Comparison between experimental data (Cummings 1996, present study) and correlations (eq. (2)).

where V_e is the onset velocity for air entrainment (Table 2) and d_1 is the jet thickness at impingement[1] Equation (2) is valid for $4.2 \leqslant x_1/d_1 \leqslant 13.2$ and $0 \leqslant (U_1 - V_e)/\sqrt{g*d_1} \leqslant 20$.

Note that several researchers observed similar correlations with circular and planar jets: i.e., for $q_{air}/q_w \propto (U_1 - V_e)^2$ for $U_1 < 2$ to 6 m/s and $q_{air}/q_w \propto (U_1 - V_e)$ at larger jet velocities (see reviews by Wood, 1991 and Chanson, 1997).

Discussion

Equation (2) is valid for supported plunging jets with partially developed inflow conditions. It may be extended to two-dimensional free jets by applying the theory of images: i.e., for a free-falling two-dimensional jet, the present data would predict:

$$\frac{q_{air}}{q_w} = 2.9E-3*\left(\frac{x_1}{d_1} - 0.52\right)*\left(\frac{U_1 - V_e}{\sqrt{g*d_1}}\right)^{1.8} \quad \text{for } V_e \leqslant U_1 \leqslant 4 \text{ m/s} \tag{3A}$$

$$\frac{q_{air}}{q_w} = 5.75E-3*\left(\frac{x_1}{d_1} - 0.52\right)*\left(\frac{U_1 - V_e}{\sqrt{g*d_1}} + 6.6\right) \quad \text{for } 4 \leqslant U_1 \leqslant 8 \text{ m/s} \tag{3B}$$

where eq. (3) is valid for $2.1 \leqslant x_1/d_1 \leqslant 6.6$ and $0 \leqslant (U_1 - V_e)/\sqrt{g*d_1} \leqslant 14$.

The quantity of entrained air may be compared with the initial free-surface aeration of the impinging jet (i.e. pre-entrainment) (Table 2, Fig. 2). At low jet impact velocity (i.e. $U_1 \leqslant 3$ m/s), the quantity of entrained air is of the same order of magnitude or smaller than the initial jet aeration. For larger jet velocities (i.e. $U_1 \geqslant 4$ m/s), the pre-entrainment accounts for only 45–65% of the total quantity of entrained air. That is, it is a substantial component of the total quantity of entrained air but the contributions of the entrapment processes by induction trumpet and air boundary layer are also significant (i.e. 35–55% of total entrained air). This last result refutes suggestions that the entrained air derives predominantly from pre-entrainment (Bin, 1993; Evans *et al.*, 1996).

4. EXPERIMENTAL RESULTS: AIR BUBBLES DIFFUSION

4.1. *Introduction*

For a two-dimensional plunging jet (Fig. 1), the air bubble diffusion process may be modelled by a solution of the advective diffusion equation. Applying a superposition method, Chanson (1997) obtained:

$$C = \frac{\frac{q_{air}}{q_w}}{\sqrt{4*\pi*D^{\#}*\frac{x - x_1}{Y_{C_{max}}}}} * \left(\exp\left(-\frac{\left(\frac{y}{Y_{C_{max}}} - 1\right)^2}{4*D^{\#}*\frac{x - x_1}{Y_{C_{max}}}} \right) + \exp\left(-\frac{\left(\frac{y}{Y_{C_{max}}} + 1\right)^2}{4*D^{\#}*\frac{x - x_1}{Y_{C_{max}}}} \right) \right) \tag{4}$$

where x is the longitudinal distance measured from the nozzle, x_1 is the free-falling jet length, y is the

[1] The jet thickness at impact d_1 was measured and also derived using the continuity and Bernoulli equations from the nozzle thickness d_0, nozzle velocity V_0 and fall height x_1. Measurements and calculations were basically equal.

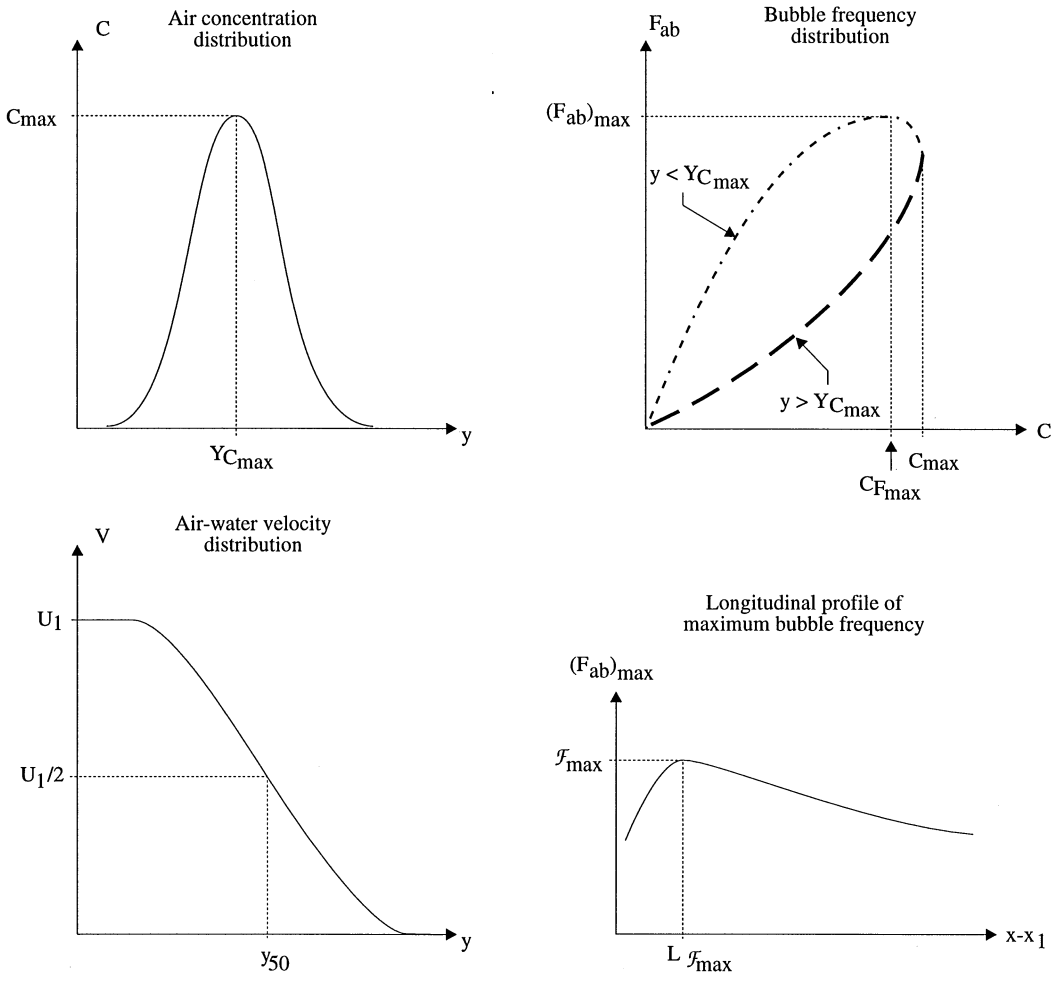

Fig. 3. Sketch of distributions of air content, air–water velocity and air bubble frequency in the developing flow region of a plunging jet.

distance normal to the jet centreline, $D^{\#} = D_t/(U_1^* Y_{C_{max}})$, U_1 is the free-stream velocity of the impinging jet, D_t is the turbulent diffusivity and $Y_{C_{max}}$ is the distance normal to the jet centreline (or normal to jet support) where the air content is maximal (i.e. $C = C_{max}$) at a given position x (Fig. 3). Equation (4) is valid in both the developing bubbly region and fully aerated flow region.

Note that the derivation of eq. (4) implies a constant eddy viscosity across the shear layer, an assumption which is certainly not true. Nevertheless, eq. (4) fits well-experimental data for a wide range of flow conditions (e.g. Chanson, 1995a, b, 1997; Cummings and Chanson, 1997a, b, Chanson and Brattberg, 1996).

4.2. *Results*

For all the investigated flow conditions, the air concentration distributions, downstream of the impingement point (i.e. $x > x_1$), exhibit the distinctive shape predicted by eq. (4) (Fig. 4). The main characteristics of the air bubble diffusion process are the maximum air concentration C_{max}, its location $Y_{C_{max}}$ and the turbulent diffusivity.

Although eq. (4) implies a longitudinal decay of the maximum air concentration in the form of: $C_{max} \propto 1/\sqrt{x - x_1}$, the experimental data are best fitted by: $C_{max} \propto (x - x_1)^{-0.44}$ for $2 \leqslant U_1 \leqslant 8$ m/s and $(x - x_1)/d_1 \leqslant 21$. For comparison, Chanson (1995a) observed previously: $C_{max} \propto (x - x_1)^{-0.59}$ with vertical supported jets ($2.4 \leqslant U_1 \leqslant 9$ m/s). Note that a similar decay of the maximum air content was also observed in hydraulic jumps with partially-developed inflow (Chanson, 1995a, b; Chanson and Brattberg, 1997).

The location of the maximum air content was observed to be independent of the jet impact velocity. Overall the data are best correlated by

$$\frac{Y_{C_{max}}}{d_1} = 0.064 * \frac{x - x_1}{d_1} + 1.19 \quad \text{for } (x - x_1)/d_1 \leqslant 21 \tag{5}$$

with a normalised coefficient of correlation of 0.966 (Fig. 5).

5. EXPERIMENTAL RESULTS: AIR–WATER VELOCITY PROFILE

5.1. *Presentation*

Downstream of the impingement point, the air–water flow is basically a free-shear layer. The characteristics of monophase shear layers were analysed in the 1920s and 1930s using the mixing length theory, and Goertler (1942) obtained the analytical solution:

$$\frac{V}{U_1} = \frac{1}{2} * \left(1 - \text{erf}\left(\frac{K^*(y - y_{50})}{x - x_1} \right) \right) \quad (6)$$

where y_{50} is the location where $V = U_1/2$ (Figs 5 and 6), K is a constant deriving from the assumption of a constant eddy viscosity ν_T across the shear layer,

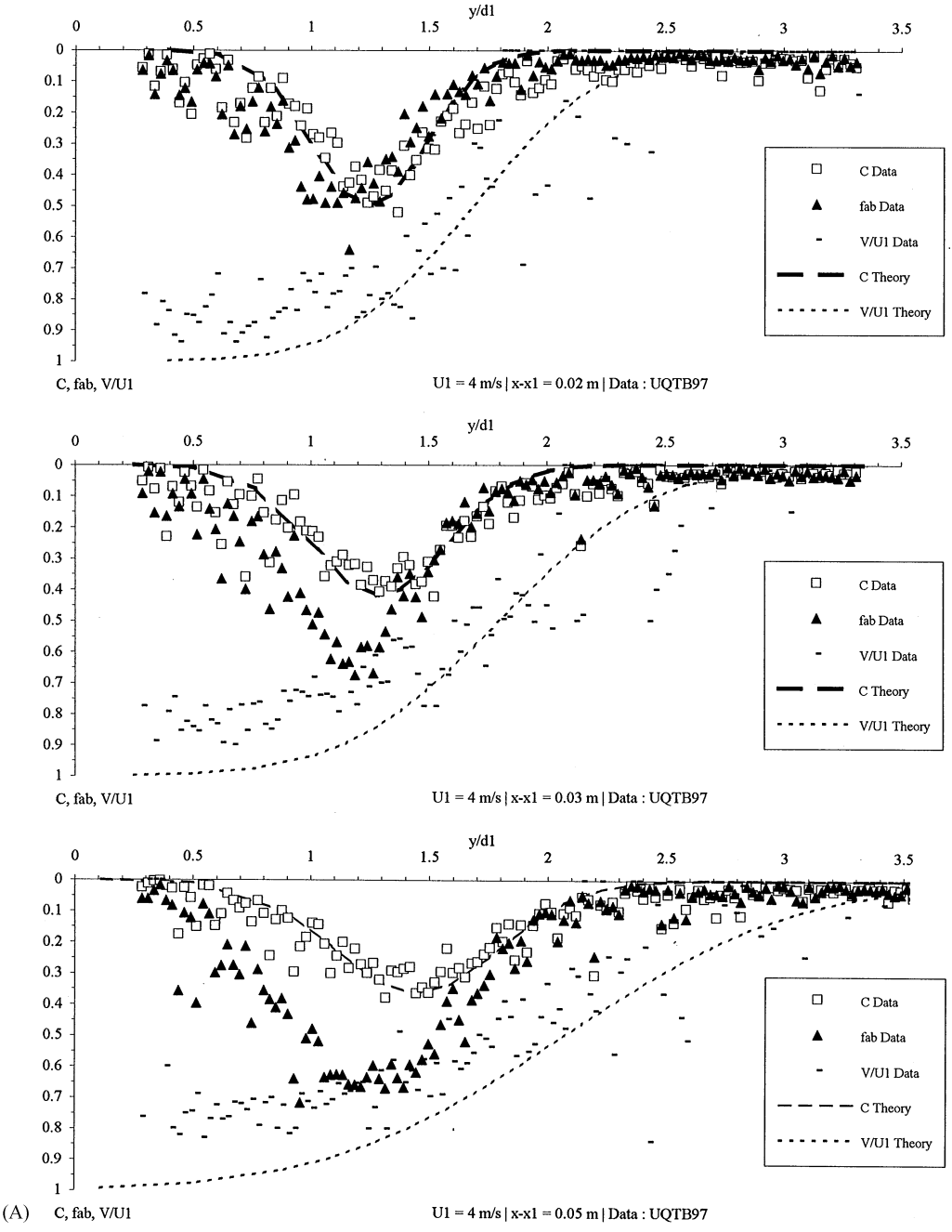

Fig. 4. Dimensionless distribution of air concentration and air–water velocity: comparison between experiments (Data: Present study) and analytical developments (eq. (4) and (6)) (A) $U_1 = 4$ m/s, $d_1 = 0.012$ m, $x_1 = 0.1$ m; (B) $U_1 = 8$ m/s, $d_1 = 0.012$ m, $x_1 = 0.1$ m.

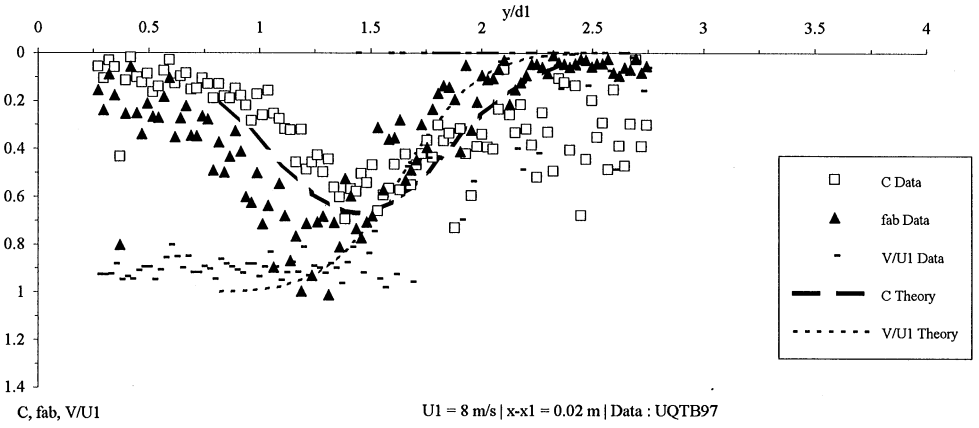

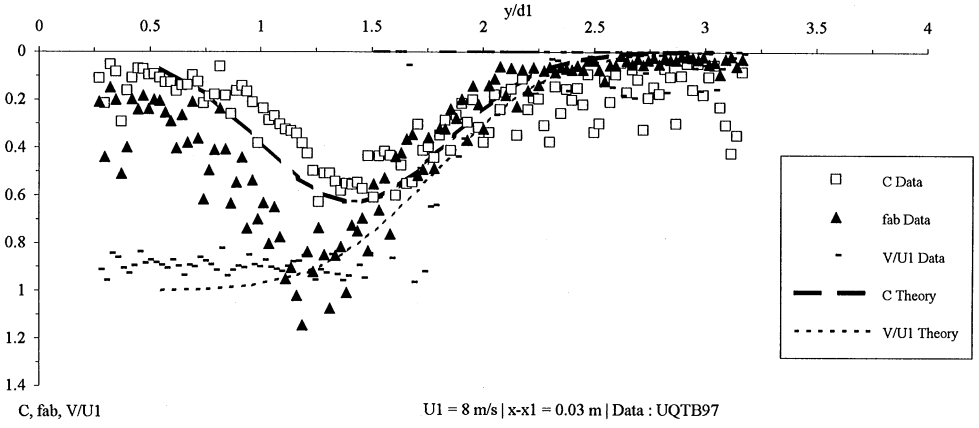

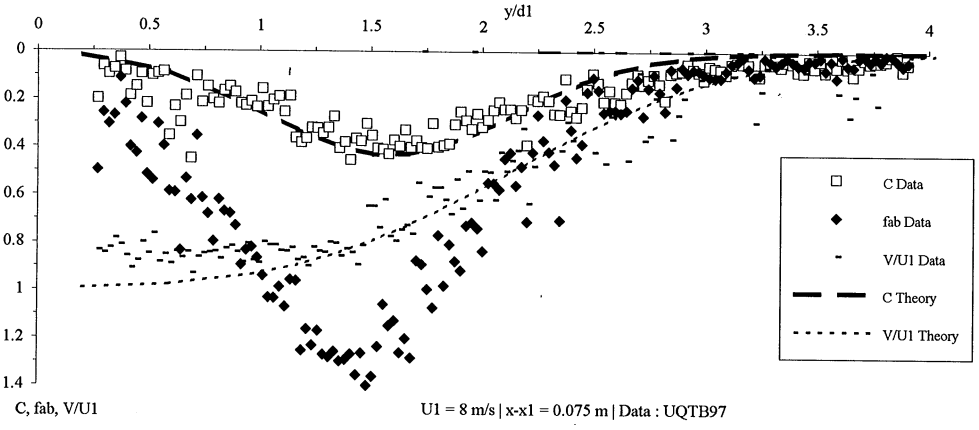

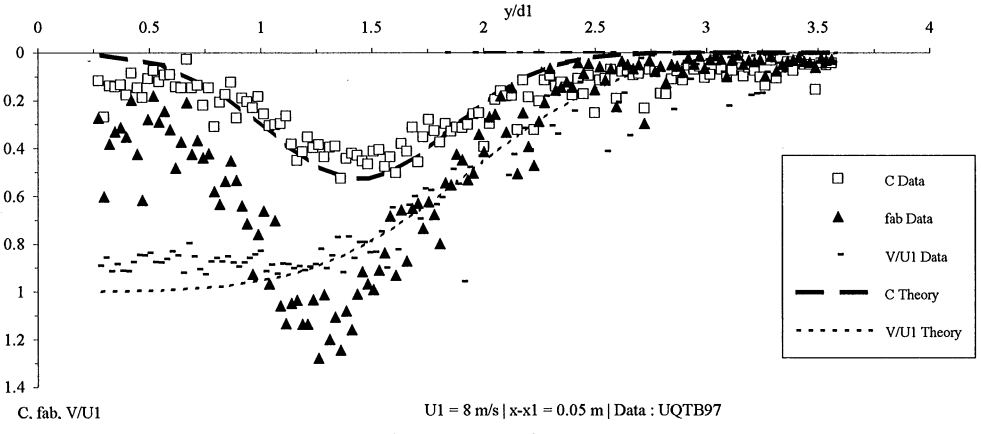

(B)

Fig. 4. *Continued.*

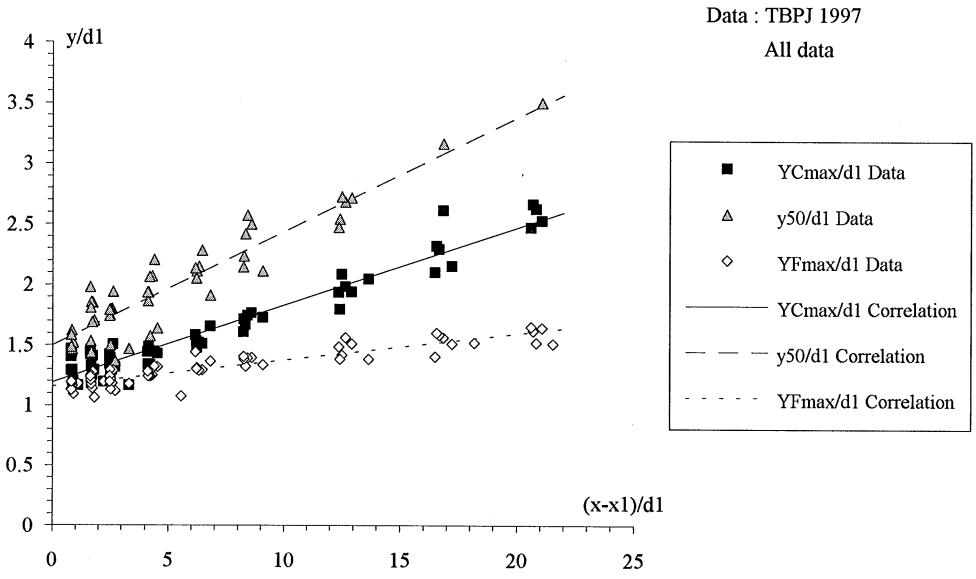

Fig. 5. Dimensionless distance from the jet support of the maximum air concentration, of the location where $V = U_1/2$ and of the maximum bubble frequency.

and the function erf is defined as

$$\text{erf}(u) = \frac{2}{\sqrt{\pi}} * \int_0^u \exp(-t^2) * dt. \quad (7)$$

The expansion rate of the momentum shear layer is proportional to $1/K$. For monophase shear layers, a generally accepted value of K is: $K = 11$ (Rajaratnan, 1976; Schlichting, 1979; Schetz, 1993).

5.2. *Air–water shear flow*

Distributions of mean air–water velocities are presented in Fig. 4. Overall the experimental results (Cummings, 1996, Present study) show consistently that the air–water velocity distributions have the same shape as in monophase shear flows: i.e. the data follow closely eq. (6). Roig (1993) observed also the same trend with low-velocity air–water mixing layers ($U_1 \leqslant 0.9$ m/s).

The early study of Cummings (1996) (see also Cummings and Chanson, 1997b) indicated further that the location y_{50} of the streamline $U_1/2$ and Goertler constant K differ significantly between monophase flows and plunging water jets. The present study investigated systematically the air–water flow properties for $2 \leqslant U_1 \leqslant 8$ m/s and the new data confirm the qualitative results of Cummings. The line of symmetry of the shear layer (i.e., y_{50}) is shifted outwards of the jet centreline (or jet support) (Fig. 5):

$$\frac{y_{50}}{d_1} = 0.094 * \frac{x - x_1}{d_1} + 1.50$$

(Data: Present study) (8)

(with a normalised coefficient of correlation of 0.945) while, for monophase flows, the following relationship holds:

$$\frac{y_{50}}{d_1} = 0.05 * \frac{x - x_1}{d_1} + 1.00$$

(Data: Wygnanski and Fiedler, 1970). (9)

The Goertler constant K was estimated from the air–water velocity data. The results (Table 3, column 4) indicate consistently smaller values of K than in monophase free shear layers. That is, the rate of expansion of the air–water shear layers is greater than that of monophase shear layers. Interestingly, the same trend was observed with low-velocity mixing layers (Roig, 1993).

5.3. *Discussion*

In the developing region of a plunging jet, the interactions between the entrained/advected bubbles and the momentum transfer across the shear layer are predominant. Cummings and Chanson (1997b) highlighted that the momentum shear layer does *NOT* coincide with the air bubble diffusion layer. This result is confirmed by the present study. The experiments show that the line of symmetry of the air bubble diffusion layer (i.e. $y = Y_{C_{max}}$) is consistently inwards of the shear layer centreline: i.e. $0 < Y_{C_{max}} < y_{50}$ at a given cross-section (Fig. 5). In simple words, most entrained air bubbles are advected in the high-velocity region of the shear layer.

Estimates of the turbulent diffusivity and eddy viscosity D_t and ν_T were determined from the best fit of the data and the results (Fig. 6, Table 3) indicate that the dimensionless turbulent diffusivity and eddy viscosity are of the same order of magnitude. For the present study the ratio D_t/ν_T increases with increasing jet velocities and becomes larger than unity for $U_1 \geqslant 5$ m/s (Table 3, column 6) because the momentum

Table 3. Air bubble diffusivity, Goertler constant K and eddy viscosity in the developing shear region of plunging water jets: experimental results

Ref. (1)	U_1 (m/s) (2)	$D_t/U_1 * d_1$ (3)	K (4)	$\nu_T/U_1 * d_1$ (5)	D_t/ν_T (6)	Remarks (7)
Cummings (1996)[a]						
2 m/s	2.39	3.92E −2	10	1.09E −2	3.59	$x - x_1 \leqslant 0.1$ m
6m/s	6.14	3.72E −2	6	2.69E −2	1.39	$x - x_1 \leqslant 0.25$ m
Present study						
TBPJ-2	2	—	5.7	5.40E −2	—	$x - x_1 \leqslant 0.03$ m
TBPJ-3	3	1.91E −2	4.9	4.82E −2	0.40	$x - x_1 \leqslant 0.1$ m
TBPJ-4-F50	4	8.67E −3	5.25	3.01E −2	0.29	$x - x_1 \leqslant 0.05$ m
TBPJ-4	4	2.74E −2	5.1	3.33E −2	0.82	$x - x_1 \leqslant 0.1$ m
TBPJ-4-F150	4	3.67E −2	6.25	2.49E −2	1.47	$x - x_1 \leqslant 0.05$ m
TBPJ-5	5	4.14E −2	4.0	4.12E −2	1.00	$x - x_1 \leqslant 0.1$ m
TBPJ-6	6	5.31E −2	6.2	3.37E −2	1.57	$x - x_1 \leqslant 0.1$ m
TBPJ-7	7	2.64E −2	6.8	2.20E −2	1.20	$x - x_1 \leqslant 0.1$ m
TBPJ-8	8	3.26E −2	7.3	1.93E −2	1.69	$x - x_1 \leqslant 0.1$ m

Notes: [a]: analysis by Chanson (1997); (—): data not available.

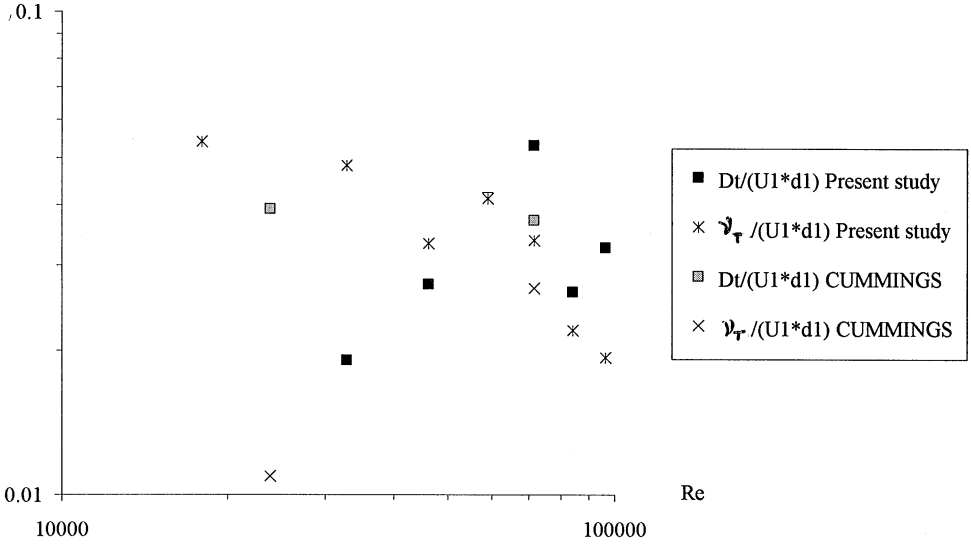

Fig. 6. Dimensionless air bubble diffusivity $D_t/(U_1 * d_1)$ and eddy viscosity $\nu_T(U_1 * d_1)$ as a function of the dimensionless velocity $\rho_w * U_1 * d_1/\mu_w$ (Table 3).

exchange coefficient ν_T tends to decrease with increasing U_1. This trend suggests that the air bubble diffusion process is dominant at larger jet velocities and that the shear layer has little effect on the air diffusion mechanism. Cummings' data gave a slightly different trend but this might be related to a lesser accuracy of the data, resulting from a different data processing technique.

6. EXPERIMENTAL RESULTS: AIR BUBBLE FREQUENCY

6.1. *Presentation*

Further information on the gas–liquid flow structure may be obtained from air bubble frequency data. Typical results are presented in Figs 7 and 8, where the dimensionless bubble frequency f_{ab} is defined as

$$f_{ab} = F_{ab} * d_1 * U_1.$$

At each cross-section, the bubble frequency distribution exhibit a characteristic shape with a maximum $(F_{ab})_{max}$ at $y = Y_{F_{max}}$ (Figs 3 and 7). Basically, the maximum bubble frequency $(F_{ab})_{max}$ increases with the inflow velocity. The position of the maximum bubble frequency is independent of the jet impact velocity and the data are best correlated by

$$\frac{Y_{F_{max}}}{d_1} = 0.0219 * \frac{x - x_1}{d_1} + 1.56 \qquad (10)$$

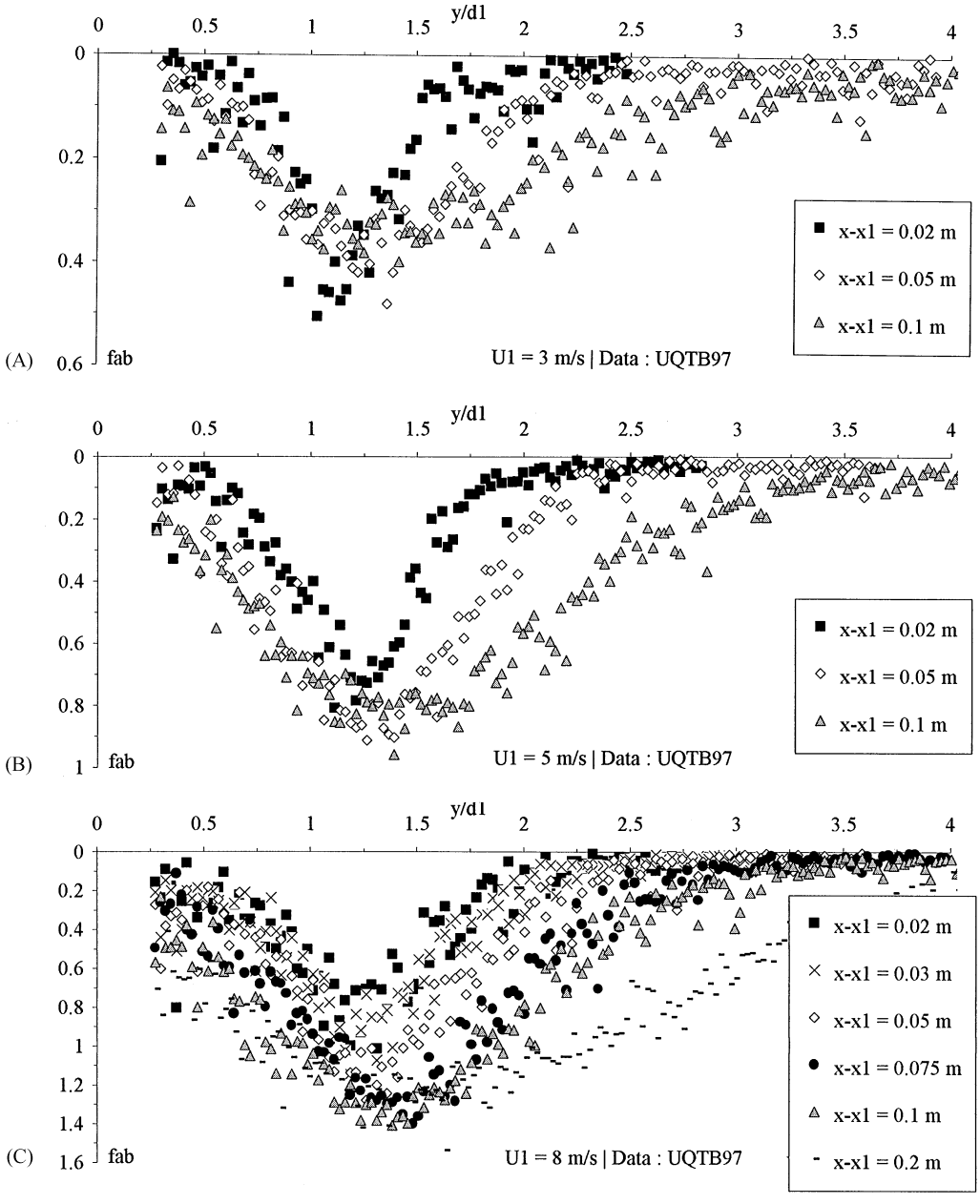

Fig. 7. Dimensionless air bubble frequency distributions in plunging jet flow. (A) $U_1 = 3$ m/s, $d_1 = 0.011$ m, $x_1 = 0.1$ m, (B) $U_1 = 5$ m/s, $d_1 = 0.012$ m, $x_1 = 0.1$ m, (C) $U_1 = 8$ m/s, $d_1 = 0.012$ m, $x_1 = 0.1$ m.

with a normalised correlation coefficient of 0.913 (Fig. 5).

Longitudinal variations of the maximum bubble frequency $(F_{ab})_{max}$ are presented in Fig. 9. For each experiment, the data (Fig. 7) indicate consistently an increasing maximum bubble frequency $(F_{ab})_{max}$ with distance $(x - x_1)$ immediately downstream of the impingement point, an upper limit F_{max}, followed by an exponential decay further downstream (Figs 3 and 9). This trend suggests that some entrained bubbles are broken up into smaller-size bubbles immediately downstream of the entrapment point $(x - x_1 = 0)$ up to the location $(x - x_1 = L_{F_{max}})$ where $(F_{ab})_{max} = F_{max}$. The result is consistent with the observations of Cummings (1996) (see also Cummings and Chanson, 1997b). For the present data, the upper limit of maximum bubble frequency F_{max} increases monotonically with the jet impact velocity and is best correlated by

$$\frac{F_{max} * d_1}{U_1} = 0.47 \, \mathrm{Ln}\left(\rho_w * \frac{U_1 * d_1}{\mu_w}\right)^{-7}$$

$$\text{for } 4E + 6 \leqslant \rho_w * U_1 * d_1/\mu_w \leqslant 6.3E + 7 \quad (11)$$

with a normalised correlation coefficient of 0.9976 where ρ_w is the water density and μ_w is the water dynamic viscosity. Note that eq. (11) was validated with air–water plunging jets only.

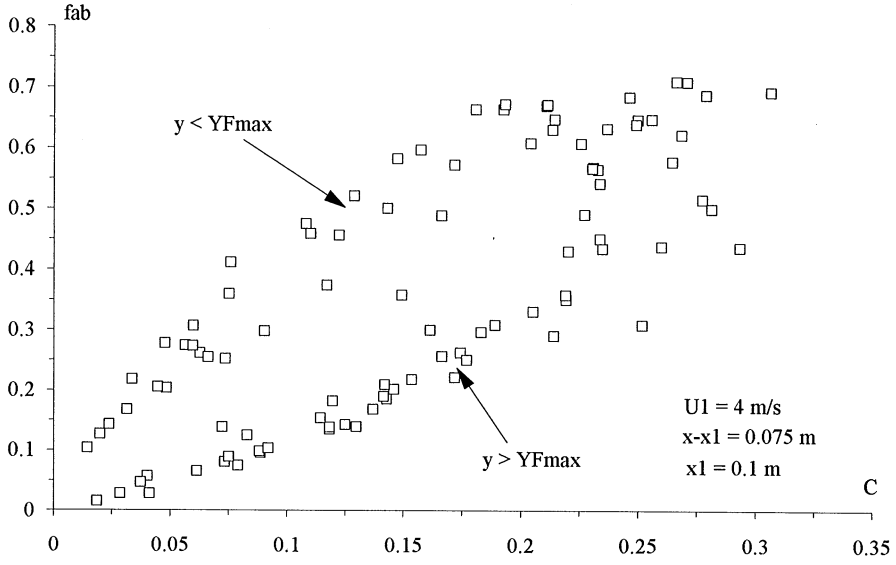

Fig. 8. Air bubble frequency as a function of the local air concentration.

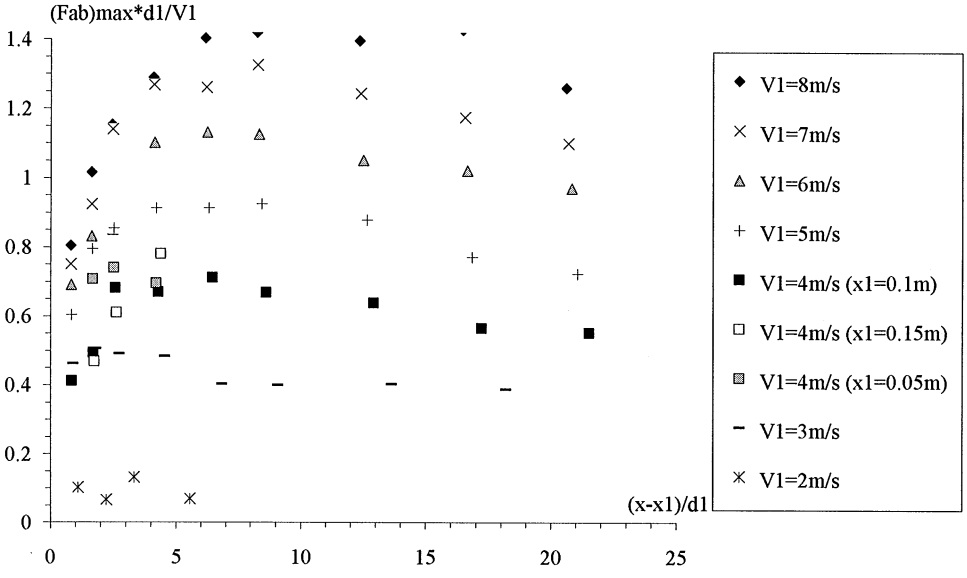

Fig. 9. Longitudinal distribution of the dimensionless maximum air bubble frequency.

Denoting $L_{F_{max}}$ the distance from the entrainment point to the location where F_{max} is observed, the ratio $L_{F_{max}}/U_1$ is a characteristic time scale of the bubble break-up process: i.e., about 10 to 20 m-s (Table 4). The senior author (Chanson) re-analysed chord length data from Cummings' (1996) study and he suggested that 'the time-scale of the entire breakage process (i.e. 'cascade' of break-ups) was typically of about 20 ms' (Chanson 1997, p. 229). Overall both analyses (Chanson 1997, Present study) produce the same conclusion: i.e. the dimensionless time scale of bubble break-up in the developing shear layer of a plunging jet is about

$$\frac{\rho_w * \sigma^2}{\mu_w^3} * \frac{L_{F_{max}}}{U_1} = 1.0 \text{ to } 4.5E + 10. \quad (12)$$

where σ is the surface tension between air and water. Note that eq. (12) is the best fit of experimental observations listed in Table 1. It characterises the time scale of the complete bubble breakup process in developing shear flow of plunging jets, rather than that of breakup of individual bubble in shear flows.

6.2. *Discussion*

For each experiment, the results show consistently that, at each cross-section x, the following relationship holds:

$$Y_{F_{max}} < Y_{C_{max}} < y_{50}. \quad (13)$$

The same relationship was observed also in the air-water shear layer of hydraulic jumps with partially

Table 4. Characteristic maximum bubble frequency F_{max}: experimental observations (Present study)

Run (1)	x_1 (m) (2)	d_1 (m) (3)	U_1 (m/s) (4)	F_{max} (Hz) (5)	$L_{F_{max}}/U_1$ (s) (6)	Remark (7)
TBPJ-2	0.10	0.0090	2.0	29.3	0.015	
TBPJ-3	0.10	0.0110	3.0	138	0.007	
TBPJ-4-F50	0.05	0.0118	4.0	245	0.019	
TBPJ-4	0.10	0.0116	4.0	250	0.008	
TBPJ-4-F150	0.15	0.0114	4.0	275	0.013	Incomplete data set.
TBPJ-5	0.10	0.0119	5.0	390	0.020	
TBPJ-6	0.10	0.0120	6.0	565	0.013	
TBPJ-7	0.10	0.0121	7.0	767	0.014	
TBPJ-8	0.10	0.0121	8.0	935	0.013	

Notes: F_{max}: upper limit of the maximum bubble frequency; $L_{F_{max}}$: distance from the entrainment point to the location where F_{max} is observed.

developed inflow conditions (Chanson and Brattberg, 1997).

For each cross-section, the air bubble frequency distribution may be presented also as a function of the air concentration (Fig. 8). The data indicate that the relationship between air bubble frequency and air concentration is not unique for $(x - x_1) \geqslant 0.02$ m (Figs 8 and 3). For $y < Y_{C_{max}}$, the bubble frequency is larger, for a given air concentration, than for $y > Y_{C_{max}}$.

In a bubbly flow, the bubble frequency, air content, mean velocity and average chord length size (i.e. number mean size) are related by

$$F_{ab} = \frac{C * V}{(ch_{ab})_{mean}}. \quad (14)$$

Equation (14) is valid for any bubble size shape, bubble size distribution and chord length distribution. Chord length data (Cummings, 1996, Present study) suggest almost constant mean chord length sizes across the shear layer (i.e., at a given cross-section, $x - x_1$ fixed). Hence the non-unique relationship between bubble frequency and air content (shown in Fig. 8) must derive from the non-coincidence between the air bubble diffusion layer and the momentum shear layer.

7. SUMMARY AND CONCLUSION

During the present study, new experiments were performed with two-dimensional supported plunging jets. The air bubble diffusion and air–water shear layer properties were investigated systematically in the near field $(0 \leqslant x - x_1 \leqslant 0.2$ m) for $2 \leqslant U_1 \leqslant 8$ m/s.

Accurate estimate of the quantity of entrained air has been deduced from the entrained air flux [eq. (2)] and the results may be extend to two-dimensional free jets [eq. (3)].

The new data confirm the qualitative findings of Chanson (1995a) and Cummings (1996). That is, in the near field, (1) the air content distributions may be modelled by an advective dispersion process, (2) the mean velocity distributions have the same shape as those in monophase shear layer but (3) the shear layer parameters (y_{50}, v_T) differ drastically between monophase and two-phase flows.

Air bubble frequency data indicate a large number of entrained bubbles. The maximum bubble frequency at each cross-section increases typically with increasing jet velocities (e.g. Table 4). For a given inflow velocity, the longitudinal distribution of maximum bubble frequency (Fig. 7) suggests some bubble breakup process next to and immediately downstream of the impingement point. The time scale of the breakup process is about 10–20 ms [eq. (12)].

The results show consistently that most entrained air is advected in the high-velocity region of the shear layer and that the locations of maximum air content, bubble frequency and shear layer centreline satisfy:

$$Y_{F_{max}} < Y_{C_{max}} < y_{50}. \quad (13)$$

Further work is required to gain a better understanding for the bubble breakup process. Additional studies of plunging jet flows are also necessary to investigate the transition region between the near-flow field and fully developed flow regions.

Acknowledgements

The authors wishes to thank Professor C. J. Apelt, University of Queensland, and Dr P. D. Cummings for their assistance and comments. They acknowledge the financial support of Australian Research Council (Ref. No. A89331591). The junior author was supported by an APA scholarship sponsored by the Australian Research Council (Ref. No. A8941296). Further the authors thank two reviewers for their helpful comments.

NOTATION

C air concentration defined as the volume of air per unit volume of air and water; it is also called void fraction

C_{max} maximum air concentration in the air bubble diffusion layer
$(ch_{ab})_{mean}$ mean chord length size, m
d jet thickness (m) measured perpendicular to the flow direction
d_0 jet nozzle thickness, m
d_1 jet thickness (m) at the impact of a supported plunging jet with the receiving pool of liquid
D_t turbulent diffusivity (m^2/s) of air bubbles in air–water flow
$D^{\#}$ dimensionless turbulent diffusivity: $D^{\#} = D_t(V_0 * d_0)$ for two-dimensional shear flow and $D^{\#} = D_t(V_0 * r_0)$ for circular jet;
f_{ab} dimensionless bubble frequency: $f_{ab} = \dfrac{F_{ab} * d_1}{U_1}$
F_{ab} air bubble frequency (Hz) defined as the number of detected air bubbles divided by the scanning time
$(F_{ab})_{max}$ maximum bubble frequency (Hz) at a given cross-section
F_{max} upper limit of maximum bubble frequency (Hz) for given inflow conditions
i integer
K integration constant in Goertler's solution of the motion equation in a shear layer flow
Ku kurtosis factor (i.e. dimensionless statistical moment of order 4) defined as:

$$Ku = \left((1/n)\sum_{i=1}^{n}(v-V)^4\right) \Big/ \times \left((1/n) * \sum_{i=1}^{n}(v-V)^2\right)^2$$

L longitudinal distance, m
$L_{F_{max}}$ distance (m) from the impingement point where $(F_{ab})_{max} = F_{max}$
n number of data points
Q_w water discharge, m^3/s
q_{air} air discharge per unit width, m^2/s
q_w water discharge per unit width, m^2/s
Sk skewness factor (i.e. dimensionless statistical moment of order 3) defined as:

$$\mathrm{Sk} = \left((1/n) * \sum_{i=1}^{n}(v-V)^3\right) \Big/ \times \left((1/n) * \sum_{i=1}^{n}(v-V)^2\right)^{3/2}$$

t time, s
Tu turbulence intensity defined as: $Tu = u'/V$; i.e., Tu is the square root of the dimensionless statistical moment of order 2: $Tu^2 = \dfrac{1}{n} * \sum_{i=1}^{n}(v-V)^2/V^2$;
u' 1-root mean square of longitudinal component of turbulent velocity (m/s) (Pitot tube data) 2- root mean square of turbulent velocity (m/s) (conical hot-film data)
U_1 free-stream velocity (m/s) of the inflow
v instantaneous velocity, m/s
V 1-velocity, m/s
2-time-averaged velocity, m/s
V_e onset velocity, m/s for air entrainment
V_0 nozzle flow velocity, m/s
W channel width, m
x distance along the flow direction, m
x_1 streamwise distance, m between the channel intake and the impingement point
y distance measured perpendicular to the channel bottom, m
y_{50} distance (m) normal to the flow direction where $V = 0.5 * U_1$
$Y_{C_{max}}$ distance (m) normal to the support where $C = C_{max}$
$Y_{F_{max}}$ distance (m) normal to the support where $F_{ab} = (F_{ab})_{max}$

Greek letters

δ boundary layer thickness, m
θ angle of the impinging jet with the horizontal
μ dynamic viscosity, Pa s
ν kinematic viscosity, m^2/s
ν_T eddy viscosity, m^2/s
ρ density, kg/m^3
σ surface tension between air and water, N/m
$\varnothing$ diameter, m

Subscript

air air flow
w water flow
1 upstream flow conditions: e.g., impinging jet flow conditions immediately upstream of impact

REFERENCES

Bin, A. K. (1993) Gas entrainment by plunging liquid jets. *Chem. Engng Sci.* **48**(21), pp. 3585–3630.

Bonetto, F. and Lahey, R. T. Jr (1993) An experimental study on air carryunder due to a plunging liquid jet. *Int. J. of Multiphase Flow* **19**(2), 281–294. Discussion: **20**(3), 667–770.

Burley, R. and Jolly, R. P. S. (1984) Entrainment of air into liquids by a high speed continuous solid surface. *Chem. Engng Sci.* **39**(9), 1357–1372.

Chanson, H. (1995a) Air bubble entrainment in free-surface turbulent flows. Experimental investigations. *Report CH*46/95, Dept. of Civil Engineering, University of Queensland, Australia, June, 368 pp.

Chanson, H. (1995b) Air entrainment in two-dimensional turbulent shear flows with partially developed inflow conditions. *Int. J of Multiphase Flow* **21**(6), 1107–1121.

Chanson, H. (1997) *Air Bubble Entrainment in Free-surface Turbulent Shear Flows*, pp. 401. Academic Press, London, U.K.

Chanson, H. and Brattberg, T. (1996) Air–water bubbly flow in free-shear layers. *Proceedings of the* 1996 *ASME Fluids Engineering Conference*, San Diego, USA, ASME-FED, Vol. 236, 1, pp. 357–364.

Chanson, H. and Brattberg, T. (1997) Experimental investigations of air bubble entrainment in developing shear layers. *Report CH48/97*, Dept. of Civil Engineering, University of Queensland, Australia, August.

Chanson, H. and Cummings, P. D. (1994a) An experimental study on air carryunder due to plunging liquid jet—discussion. *Int. J. of Multiphase Flow* **20**, (3), 667–770.

Cummings, P. D. (1996) Aeration due to breaking waves. Ph.D. thesis, Dept. of Civil Engng, University of Queensland, Australia.

Cummings, P. D. and Chanson, H. (1997a) Air entrainment in the developing flow region of plunging jets. Part 1. Theoretical development. *J of Fluids Engng*, *Trans. ASME* **119**, 3, 597–602.

Cummings, P. D. and Chanson, H. (1997b) Air entrainment in the developing flow region of plunging jets. Part 2. Experimental. *J of Fluids Engng*, *Trans. ASME* **119**, 3, 603–608.

Evans, G. M., Jameson, G. J. and Rielly, C. D. (1996) Free jet expansion and gas entrainment characteristics of a plunging liquid jet. *Exp. Thermal Fluid Sci.* **12**(2), 142–149.

Goertler, H. (1942) Berechnung von aufgaben der freien turbulenz auf grund eines neuen näherungsansatzes. *Z.A.M.M.* **22**, 244–254 (in German).

McKeogh, E. J. and Ervine, D. A. (1981) Air entrainment rate and diffusion pattern of plunging liquid jets. *Chem. Engng Sci.* **36**, 1161–1172.

Rajaratnam, N. (1976) Turbulent Jets. Development in Water Science Vol. 5. *Elsevier Scientific Publ. Co.* New York, U.S.A.

Roig, V. (1993) Zones de Mélange d'Ecoulements Diphasiques à Bulles. ('Two-Phase Bubbly Mixing Layers.') Ph.D. thesis, INP Toulouse, France, No. 714, May, 349 p (in French).

Schetz, J. A. (1993) *Boundary Layer Analysis.* Prentice Hall, Englewood Cliffs, NJ, U.S.A.

Schlichting, H. (1979) *Boundary Layer Theory*, 7*th edn.* McGraw-Hill, New York.

Sene, K. J. (1988) Air entrainment by plunging jets. *Chem. Engng Sci.* **43**(10), 2615–2623.

Van de Donk, J. (1981) Water aeration with plunging jets. Ph.D. thesis. TH Delft, The Netherlands, 168 pp.

Van de Sande, E. and Smith, J. M. (1973) Surface entrainment of air by high velocity water jets. *Chem. Engng Sci.* **28**, 1161–1168.

Wood, I. R. (1991) Air entrainment in free-surface flows. *IAHR Hydraulic Structures Design Manual No.* 4, Hydraulic Design Considerations. Balkema Publ., Rotterdam, The Netherlands, 149 pp.

Wyganski, I. and Fiedler, H. E. (1970) The two-dimensional mixing region. *J. Fluid Mech.* Part 2 **41**, 327–361.